Structural characterization of Propylammonium nitrate and N-methyl-2-Pyrrolidone mixtures

E. Scarpellini[a,*], M. Usula[b], R. Caminiti[a]

[a] *Dipartimento di Chimica;Universitá di Roma "La Sapienza"; Piazzale A. Moro 5, I-00185, Roma*

[b] *Dipartimento di Scienze Chimiche e Geologiche, Universitá degli Studi di Cagliari, S.S. 554 Bivio Sestu, 09042 Monserrato, Italy*

Abstract

Propylammonium nitrate (PAN) ionic liquid and *N*-Methyl-2-pyrrolidone (NMP) are well know compounds employed for many applications in different industrial fields. The most interesting feature is the possibility of modulating the structural properties of the ionic liquid by mixing it with the molecular solvent. A dynamic characterization of the PAN-NMP mixtures is desirable to understand the significant effects on the structural properties and consequently on the chemical-physical features induced by the formation of such solutions. In order to improve the knowledge of the structure of PAN-NMP solutions, useful to the development of their applications, Energy dispersive X-ray diffraction (EDXD), and molecular dynamics (MD) simulations were employed in this work. Our study evidenced a microeterogeneous solvation of PAN by NMP and indicate the presence of strong attracting interactions between the constituents.

Keywords: ionic liquid, Propylammonium nitrate, N-Methyl-2-pyrrolidone, x-ray diffraction, MD simulation

1. Introduction

Room-temperature ionic liquids (RTILs) belong to the class of organic salts liquid at room temperature. At the present time the number of RTILs

*Corresponding author

Email address: eleonora.scarpellini@uniroma1.it (E. Scarpellini)

synthesized exceeds 500 and research in this area is expanding rapidly. Because of their features such as non-volatile nature and good solvation properties, RTILs attract much attention as a valid alternative to traditional volatile organic solvents [1, 2, 3]. The unique properties of RTILs are determined by the structure and interaction between ions: they are usually composed of large asymmetric organic cations and inorganic or organic anions. Besides RTILs can be divided into two groups: protic (PILs) and aprotic (AILs) ionic liquids. The acid proton, which is responsible for hydrogen bonding, makes PILs different from other ionic liquids and suitable for different potential applications, such as self-assembly media, catalysts in chemical reactions, biological applications [4]. In order to use RTILs as solvents, it is necessary to be able to predict their behavior in terms of their miscibility with other solvents. Experimental and/or theoretical thermodynamic studies on pure RTILs and their mixtures with organic solvents or water were reported in [5, 6]. Furthermore Heintz [7] reviewed the developments of thermodynamic and thermophysical studies of RTILs + non-aqueous solvent mixtures including an overview on the experimental data available. The review is limited to systems having the most promising chance to be used successfully in the different fields of chemistry and chemical engineering. Characterization of mixtures containing ionic liquids and organic solvents is needed to test their applicability in substitution of neat compounds which could have inappropriate properties for a selected application, i.e. limited solvent power range or high viscosity [6]. Propylammonium nitrate (PAN) is one of the most known PILs and its properties make it suitable for electrochemical, organic, or biochemical applications [4]. For example it is used as solvent/catalyst in organic reactions leading high yields. On the other side, *N*-methyl-2-pyrrolidone (NMP) is an organic solvent known for its low toxicity, low volatility and high solvent power and it is becoming the product of choice for paint strippers, agricultural chemicals, and process solvent applications. Recently, different studies have pointed out the interesting properties of NMP with water [8]. Despite PAN and NMP have been the subject of a lot of studies, either as pure compounds or in mixture, results of structural features of their solutions have not been reported in the literature until now. In this work, PAN, was selected with the aim to investigate its behavior when mixed with NMP. Seven solution were prepared covering the whole concentration range, with the purpose of understanding the structural interactions that occur during mixing.

2. Materials and Methods

2.1. Materials

PAN was purchased from Iolitech (97% purity) and NMP from SigmaAldrich (97% purity). Before use, all materials were dried in vacuo ($p = 7 \cdot 10^{-1} mbar$) for 48 h at room temperature. The PAN + NMP mixtures were prepared by mass as follows: the proper amounts of PAN and NMP were weighted with an analytical balance (Sartorius A210P, DataWeighing Systems Inc. IL-USA; precision and accuracy of $\pm 1 \cdot 10^{-7} kg$ and $\pm 5 \cdot 10^{7} kg$, respectively) in screw-cap glass vials in a glove-bag under nitrogen atmosphere. For density determinations, PAN and NMP were degassed for about 2h by means of an ultrasonic device (WVR model USC100T -45kHz, 30W). The residual water content of NMP and PAN, was estimated by ^{1}H NMR spectroscopy by using VarianUnity INOVA 500 spectrometer operating at the proton resonance frequency of 499.84 MHz, and resulted to be χ_{WAT} <0.02 per mole fraction. In Table 1, the mixture composition expressed as PAN mole fraction (χ_{PAN}), molar ratio (R) between moles of PAN and NMP and experimental densities from [8] are reported for the seven prepared solutions. The table also reports the MD simulations details (such as the numbers of NMP and PAN molecules in the simulation box) that will be discussed later in the text.

2.2. X-ray diffraction

The large angle X-ray scattering experiments were performed at room temperature using the non-commercial energy scanning diffractometer built in the Department of Chemistry at the University La Sapienza of Rome (Italian Patent No. 01126484-23 June, 1993). In this experiment, the new 0-2θ instrument geometry (only one of the two diffractometer arms can move) was used; the samples were prepared and put in 2 mm quartz cylindrical capillaries, immediately after a 72 h drying in high vacuum pump. In such setup, higher diffracted intensities can be recorded. The diffraction patterns acquired at the different angles were then joined to obtain a continuous spectrum in Q [9, 10]; **the variable Q is the magnitude of the transferred momentum and depends on the scattering angle (2θ), wavelength (λ), and energy (E) of source, according to the relation** $Q = 4\pi(sin\theta/\lambda) = cost \cdot E \cdot sin\theta$**, with cost ≈ 1.0136, if E is expressed in keV and Q in Å^{-1}.** Only five diffraction angles are enough to cover a Q-spectrum ranging from 0.1 to 20 Å^{-1}. Consequently, the total intensity of the radiation scattered by the sample, $I(Q)_{e.u.}$, is a function of Q. The

measured $I(Q)_{e.u.}$ is hence corrected for systematic effects (polarization, absorption, and incoherent scattering) and rescaled to absolute units (electron units per stoichiometric unit). It can be also expressed as the sum of the independent atomic scattering from the atoms in the stoichiometric unit, and by $i(Q)$, the *total (static) structure factor*. The $i(Q)$ function constitutes the structurally sensitive part of the scattering intensity being due to the interference contributions from different atoms. In fact it is related to the *radial distribution functions*, $g_{ij}(r)$, descriptive of the structure, according to the formula:

$$i(Q) = \sum_{i,j=1}^{m} x_i x_j f_i f_j H_{ij}(Q) \tag{1}$$

where x_i are the numerical concentrations of the species, and f_i are their Q-dependent X-ray scattering factors. H_{ij} is the partial structure functions and it is defined by the Fourier integral [11]:

$$H_{ij}(Q) = 4\pi\rho_0 \int_0^\infty r^2 \cdot \big[g_{ij}(r) - 1\big] \cdot \frac{sin(Qr)}{Q} \quad dr \tag{2}$$

(ρ_0 is the bulk number density of the system).
Therefore, through computed radial distribution functions, is possible to obtained a theoretical $i(Q)$ function which can be compared with the one that derive from experimental diffraction patterns $I(Q)_{e.u.}$. **Both the experimental and theoretical $i(Q)$ were multiplied by a modification function $M(Q)$:**

$$M(Q) = \frac{f_N^2(0)}{f_N^2(Q)} \cdot exp^{-0.01Q^2} \tag{3}$$

this function also know as "sharpening factor", is necessary to improve the curve resolution at high Q. N is Nitrogen, a second-period element used as a typical "sharpening atom". The *static structure factor*, both experimental and theoretical, is finally expressed as $Qi(Q)M(Q)$ and the effect of $M(Q)$ can be seen on Ref. [12]. The $M(Q)$ is useful to obtain a more resolved Fourier-transformed into the *differential correlation function* Diff(r), according to the relation:

$$\mathrm{Diff}(r) = \frac{2r}{\pi} \int_0^\infty Q \cdot i(Q) \cdot M(Q) \cdot sin(Qr) \quad dQ \tag{4}$$

which contains only the structural contribution to the distribution fuction. All the functions were calculated using in-house written codes (L. Gontrani

and R. Caminiti, *private communication*). All the above functions were calculated from the MD trajectories using in-house codes purposely written (L. Gontrani, *private communication*). For a comprehensive report of all the formulas, see Ref. [13].

2.3. Simulation Details

The molecular dynamics simulations were performed with the AMBER 11 package [14] (both CPU and GPU versions of PMEMD) using a cubic box. Geometry and atom numbers are reported in **Figure 1**. The box edge and

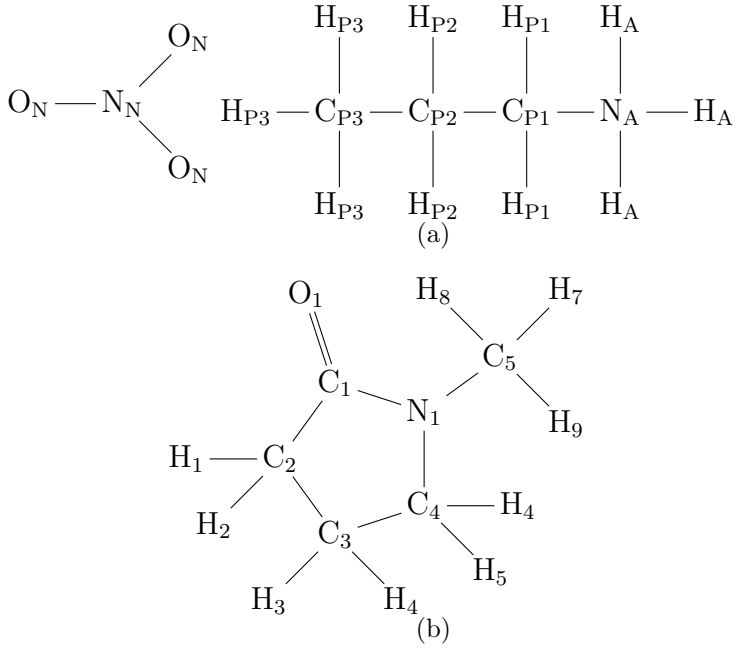

Figure 1: *Atom numbering scheme of (a) propylammonium nitrate and (b) N-methyl pyrrolidone.*

the number of molecules were optimized basing on the measured density of the liquid at 25 $^{\circ}C$ (see Table 1) and according to the criteria of periodic boundary conditions: to fully reproduce the spatial correlations observed in the experimental spectra, a box whose edge is at least twice the distance corresponding to the last peak of experimental radial distribution function was used. The energy of the system was modeled with the two-body generalized AMBER [14, 15] force field GAFF, using standard Particle Mesh Ewald

(PME) treatment of electrostatic interactions under periodic boundary conditions; all the bonds involving hydrogen atoms were constrained using the SHAKE algorithm. A cutoff of 8.0 Å was used for both intermolecular interactions (treated with **Lennard-Jones 6-12** potential) and the real part of Ewald sum. The standard Lorentz-Berthelot combination rule was used for all the unlike atom types. Every atom of the molecule defines a distinct atom type, even if the parameters are equal (as, it happens, for instance, for hydrogen atoms or C_2 and C_3). The partial atomic charges were fixed throughout the simulation and were obtained according to the Restrained Electrostatic Potential (RESP) procedure,by fitting the electrostatic potential calculated on the *ab initio* optimized molecular structure [16]. Thus the structure of PAN and NMP molecule was optimized at the HF/6-31G(d) quantum-mechanical level[17]. The use of such quantum-mechanical (QM) level in the charge calculation is justified by the larger value of the dipole moments that are obtained with this method (about 20 % more than *in vacuo* experimental values, so that the charges resulting from the fitting are higher in value (pre-polarized). In this way, the charge polarization expected in condensed phase induced by many body effects can be partially accounted for using this effective two-body approach [18, 19]. Afterwards the simulation cell was filled with the number of geometry-optimized NMP and PAN molecules required by composition/density with the software PACKMOL [20] using a minimum interatomic separation of 2 Å as the only constraint; the relative ratio between PAN and NMP molecules is reported in Table 1. The box was subject to 10000 cycles of conjugate-gradient energy minimization and a short NVT run (10 ps) at 50 K was carried out to prevent the formation of vacuum bubbles in the system. Then the system was heated to 300 K in a step-wise manner (with steps of 2 K each), for a total of 100 ps. A dynamics of 400 ps in the NPT ensemble was hence performed. This is adequate to lead the box equilibration to a density that does not differs from the measured value by about 1.26%. The procedure has proved valid for the simulation of NMP neat liquid [21]. Furthermore considering that a NVT production run was planned afterwards, no further box equilibration was performed. Therefore a 4 ns trajectory was then produced in the NVT ensemble (at the experimental density), with integration time step of 1 fs.

Sample	χ_{PAN}	R (n_{NMP}/n_{PAN})	*Density experimental* (g/cm^3)	*NMP molecules*	*PAN molecules*
PN005	0.05	15.93	1.04163	1593	100
PN012	0.12	8.32	1.04865	832	100
PN033	0.33	2.48	1.07303	744	300
PN05	0.5	1.38	1.08954	690	500
PN064	0.64	0.67	1.10927	402	600
PN087	0.87	0.32	1.12489	224	700
PN095	0.95	0.02	1.14387	20	1000

Table 1: ***For each investigated PAN+NMP mixtures and simulation system: acronym of the solution; PAN mole fraction; molar ratio between PAN and NMP moles (R); experimental density at 25°C; number of NMP and PAN molecules used for each simulation box based on concentration ratio R.***

3. Results and Discussions

The first relevant result that can be extracted form our trajectories is the static structure factor. This quantity, which provides us of a general idea of the liquid structure, can be used as a probe of the accuracy of the calculations when directly compared to the experimental measurement. Here it is presented a comparison of the X-ray static structure factor $QM(Q)i(Q)$ calculated from the MD simulations and the corresponding experimental measurement in the *upper panel* of **Figure 2** for the PN005 sample as example. All the consideration are valid for all the others mixture. A complementary quantity that can help in the understanding of the liquid structure is the Diff(r) function as calculated through Eq. 4. This quantity is presented in the *lower panel* of Figure 2. As it can be easily seen from Figure 2 most of the important features are actually very well described at the classical level even if we are using a general force field with static charges. The overall agreement between the experimental and simulation data is good, for all distance and Q ranges. Such agreement indicates that this model is reliable and appropriate to gather structural information about the mixture.

3.1. Structure

The structure functions show broad peaks typical of liquids, with a moderate degree of order suggested from intensity. The assignment of peaks in reciprocal space is not directly feasible since more structural correlations of the various diffraction centers contribute to each peak. But is reasonable to

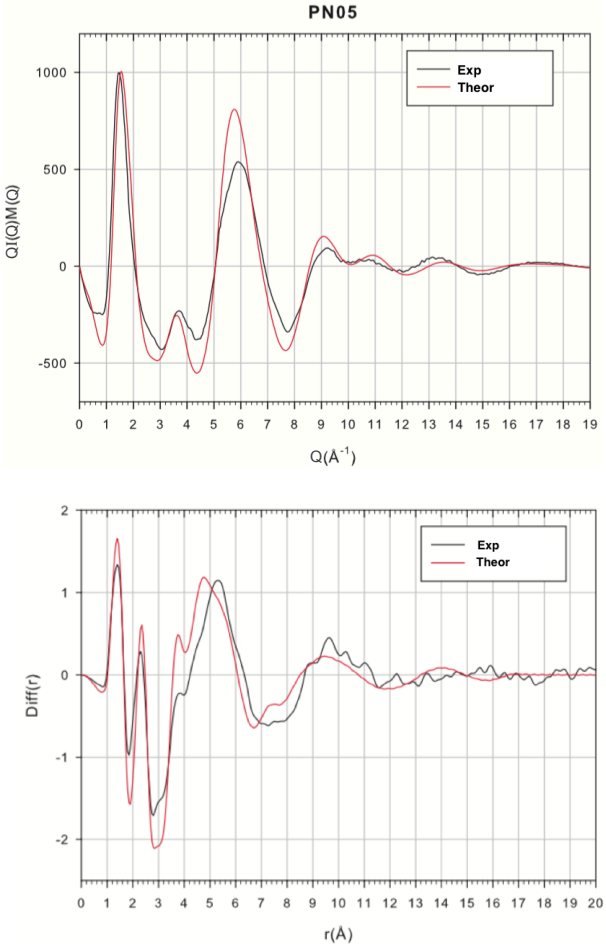

Figure 2: *upper panel*: PN005 mixture sample QI(Q)M(Q) experiments (black) and theory (red). *lower panel*: the Fourier transform of the QI(Q)M(Q) data gives rise to the Diff(r) function.

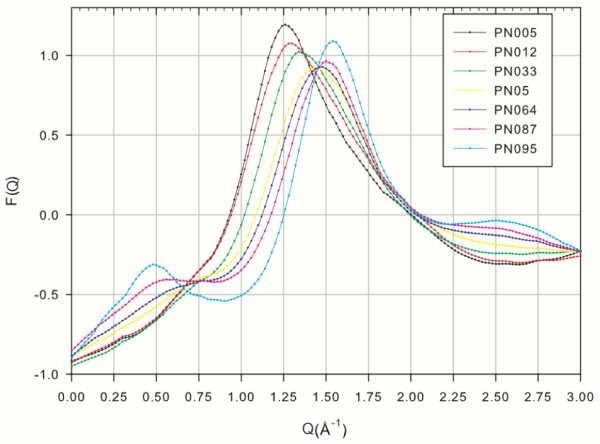

Figure 3: *First peak of structure functions for each sample.*

Sample	*i(Q)* first peak (Å^{-1})
PN005	1.28
PN012	1.32
PN033	1.40
PN05	1.46
PN064	1.52
PN087	1.54
PN095	1.56

Table 2: *Q value of structure function first peak of each sample.*

say that *intramolecular* scattering are responsible for at least all the intensity observed **above** 2 Å^{-1}, while the *intermolecular* contacts originate the main peaks that fall between 1.28 and 1.56 Å^{-1}. The Q-positions of the first peak on the structure function that corresponds to the intermolecular contacts are collected in Table 2 for all the mixtures. A direct comparison of the first intermolecular peak of all samples is shown in Figure 3. Since each sample have different composition, it is necessary to normalize the structure functions for concentration and scattering factors, using functions calling *atomic funcions* or $F(Q)$, normalized for the number of atoms x_i and the scattering factors f_i:

$$F(Q) = \frac{i(Q)}{\sum_i x_i f_i^2}$$

$F(Q)$ ranges between 1 and -1, and therefore allows to directly compare the curves of all the samples, which instead would not be possible because of the different intensity. In this figure it is clearly possible to see the peak shifts to values of increasing Q. The peak of the first sample, the most diluted PAN mixture (PN005), falls to 1.28 Å^{-1}, exactly the same pure NMP value [21]. This is not surprising since the quantities of ionic liquid in the solution is really poor, just 0.607 moles, with a ratio of 15 NMP molecules to one PAN. The value of Q-peak gradually increases with decreasing concentration of NMP up to 1.56 Å^{-1}. From the structure functions, in addition to the progressive peak shift, also the variation of its intensity is observed. The first and the last sample have narrower and more intense signals (more

"crystalline") since the compounds are "almost pure". The other mixtures have instead low and broad peaks because of contain additional intermolecular interactions between the two species. Furthermore, in Fig. 3 it could be noticed that a little peak appears at ca. 0.5 Å before the main one as the samples progressively get richer in PAN. These are called "pre-peaks" or "peaks at low Q" or "FSDP-first sharp diffraction peak" whose presence, recognized in aqueous solutions of metal ions and ionic liquids is generally attributed to the existence in the liquid of a considerable medium range order (greater than 10-20 $Å^{-1}$) [22, 23, 24]. **This behavior is confirmed from the simulated $F(Q)$ as calculated on the NVT MD trajectories (see Figure 4), in which it turns out clear that the appearance of the low-Q peak occurs in the sample with the highest concentration of the ionic liquid.** As already mentioned, the structure function after 2

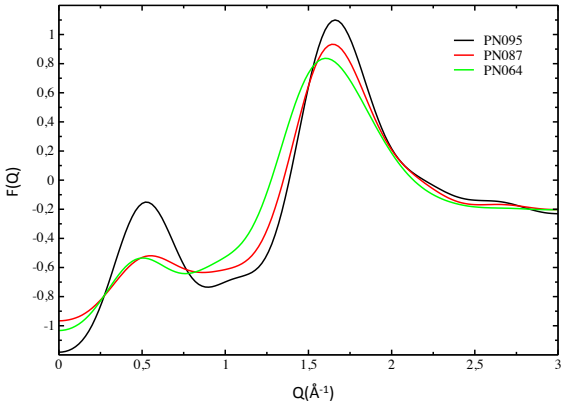

Figure 4: *First peak of structure functions for samples with PAN molar fraction equal to 0.64 (PN064), 0.87 (PN087), 0.95 (PN095)* ***as extracted from MD trajectories in NVT ensambles, neglecting the first 500 ps of simulation.***

$Å^{-1}$ presents intramolecular peaks, a sort of fingerprinting of the molecule. This aspect is confirmed by several structural studies on protic ionic liquids [25, 26, 27]. As regards the Diff(r) function (see **Figure 5**), the first qualitative information supplied is the considerable long range order present in these solutions. After two net molecular peaks attributed to atoms directly linked and after the intramolecolar contacts 1-3, there are three to four *intermolecolar* "shell" as the solution enriches in PAN. This is in agreement with the presence of the main peak below **2 $Å^{-1}$** in the structure functions,

typical of long period order. The appearance of a shoulder around 3-3.5 Å in the Diff(r) function can also be notice, that is regarded as the fingerprint of the ion pair. The spatial correlation of the system quickly decays after 17 and the signal becomes indistinguishable from noise. A detailed analysis of the differential correlation functions is presented further in the text.

3.2. Peak assigment

The assignment of the peaks is possible only on the direct space, thus analyzing the radial distribution functions or, as in this case, the differential correlation functions. *Intramolecular* contacts can be easily identified in the curves reported in **Figure 5**, since the corresponding peaks are very prominent (i.e., there is high structural correlation=low variability in the value of the distance); on the other hand *intermolecular* interactions give origin to larger and low intensity peaks. As already anticipated in the qualitative discussion, the first peak of Diff(r) contains the contributions of bonded atoms; the second peak, contains 1-3 intramolecular contacts. Table 3 shows the values of r of the first two peaks (intramolecular contacts) on Diff(r) curves of the seven solutions. The position value of the first two peaks tends to decrease, even if slightly, indicating that the distances are shortened passing from the cyclic ring of NMP to the alkyl chain of the PAN. The observed shift of the two main peaks at the values of 1.25 and 2.10 Å for the first and for the second one, correspond, respectively, to the typical bond distances of N_N-O_N and O_N-O_N of nitrate. As for subsequent interactions is necessary to analyze the various mixtures separately. As shown in Figure 5 the first two PN005 and PN012 samples, with a high concentration of NMP, show a Diff(r) very similar between them and immediately attributable to the function of the pure liquid. For distances 1-4 it is possible distinguish a *cis* and *trans* arrangements. The first case (distance O_1- C_5 of NMP) produces a weak shoulder around 3 Å while the distances C_5- C_2, C_5-C_3, O_1-C_4, and O_1-C_3 give a peak around 3.8 Å. Beyond the well at 3.2 Å, a range of distance where both *intra* and *intermolecular* correlations contribute is entered. However, *intramolecular* peaks can be identified since they give rise to shoulders. In addiction to the case already cited (the 3.8 Å peak), two shoulders still have contributions of *intramolecular* origin: the first one, falling around 4.2 Å, contains 1-5 contacts (such as O_1-H_5), while the last one (around 4.85Å) by 1-6 interactions between far hydrogen atoms, (such as H_8-H_3), although the intensity of such interaction is small, given the low x-ray scattering amplitude of hydrogen atoms. The first *intermolecular* peak is about at 6 Å followed

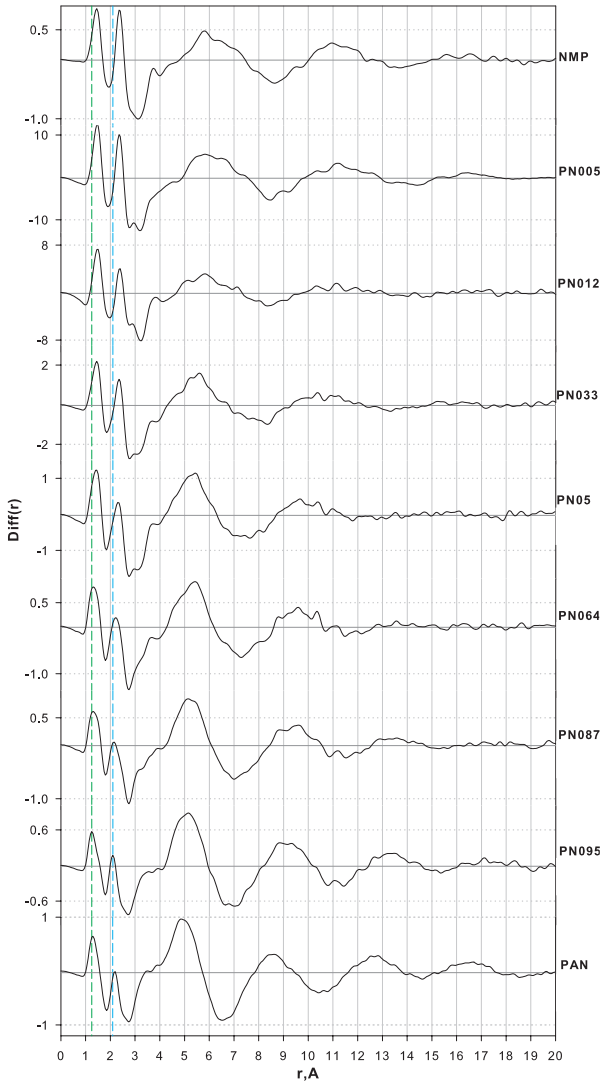

Figure 5: *Differential correlation functions (Diff(r)) of the neat compounds and their mixtures at different concentrations. The green and blue line help to follow the peak shift. Both functions for NMP and PAN pure liquid is also reported for a direct comparison with those of solutions.*

by a second shell of solvation. The PN033, PN064, and PN05 mixtures are gradually enriched with PAN, consequently the Diff(r) gradually becomes

more structured. The shoulder around 3 Å (O_1-C_5 bond of NMP) disappears (already not seen in PN064) while the next peak shoulder including the distances of 1-4 PAN grow up.

Sample	First peak (Å)	Second peak (Å)
PN005	1.45	2.35
PN012	1.45	2.40
PN033	1.45	2.30
PN05	1.40	2.30
PN064	1.30	2.20
PN087	1.25	2.15
PN095	1.25	2.10

Table 3: *Distance (r) of first and second peak of the Diff(r) for each PAN-NMP mixture at different composition.*

The shoulder falling around 3.8 Å persists although it tends to lower values reaching ca. 3.5 Å. In fact, this value corresponds to the interaction between the ion pair, and it falls within the range in which the distances are still *intramolecular*. Instead, the shoulder around 4-5 Å disappears and the contacts 1-5, 1-6 fall in the *intermolecular* first peak region that has a maximum around 5.5 Å (shorter than in pure NMP). Then it is possible to see a solvation shell around 10 Å. The two remaining samples PN087 and PN095, very rich in PAN, tend to take the form of the pure liquid curve. The wide shoulder between 3 and 4.2 Å includes all 1-4 and 1-5 *intramolecular* contacts of propylammonium nitrate, as well as the *intermolecular* distances between the ion pair. The next peaks with a maximum at 5.5, 9, 13 and **16.5 Å** correspond to four *intermolecular* shell. The presence of a third shell is compatible with samples formed almost exclusively by ionic liquid, organized according to a structure which located an alternation between ions of opposite sign. For a better understanding of the sistem, the evolution of the *partial differential correlation curves* "$\mathrm{Diff_{ij}}$" is qualitatively analyzed. For all the configurations saved in the trajectory, both partial radial distribution functions g_{ij} and their Fourier transform H_{ij} (Eq. (2)) were calculated. To facilitate this analysis, we calculated, starting from the simulation $g_{ij}(r)$ normally obtained from the trajectory for every pair of atom types, a partial "Diff(r)" distribution curve, in order to confront curves with the same functional form. These functions are obtained by the equation:

$$\mathrm{Diff_{ij}}(r) = 4\pi r^2 \rho_0 (g_{ij}(r) - 1) \tag{5}$$

Partial $\mathrm{Diff_{ij}}(r)$ of N_A-O_N (i is N_A and j is O_N) is reported in Figure 6. It could be noticed that theoretical patterns are limited to half the value of the simulation box size, and that the curves are shifted to facilitate comparison. The Figure 6 show the predict correct average distance between the O_N acceptor and the N_A donor (2.9-3 Å), and it is also visible a second shell around 4.6-4.9 Å. The *intermolecular* N_A-O_N contacts (between propylammonium

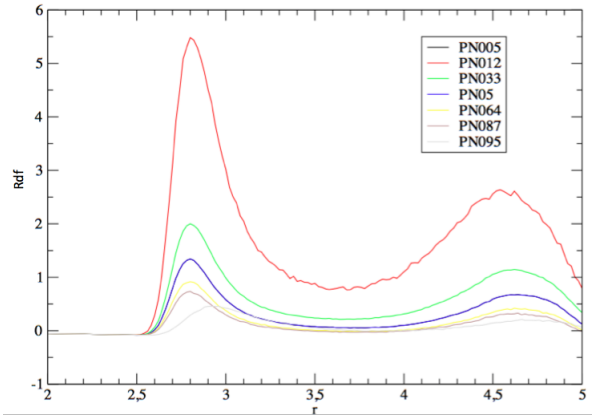

Figure 6: *Radial distribution function of N_A-O_N for each mixture* ***as obtained by MD simulations of the investigated systems in NVT ensamble neglecting the first 500 ps of the respective trajectories.***

and nitrate ions) is rather short. Also the N_A-O_1 distances (not shown here) falls at 2.8 Å and 4.4 Å (in line with those reported in other studies for methylammonium nitrate compounds). All other interactions have larger distances. It may be assumed that the interactions between the N_A , O_N and O_1 atoms is primarily responsible for the cohesion of the liquid and that propyl cations, ammonium anions, and the NMP molecules are interchangeable, forming an alternating structure.

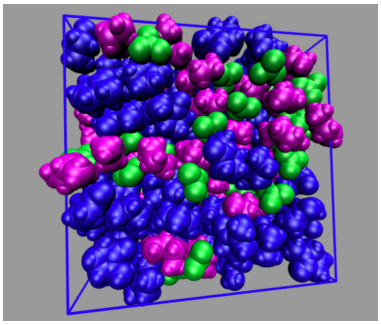

Figure 7: *Frame of simulation box of PN05 solution. Blue*, NMP. *Green*, nitrate of PAN. *Pink*, propylammonium of PAN

On the other hand the coulombic interaction between propylammonium and nitrate ions shows an higher strength than the *intermolecular* interaction between the propyl and NMP molecules. A general result, although quite obvious, is that the correlation within the ion pair is stronger than those between the propylammonium molecule and NMP. In the PAN-rich mixtures, PN095 and PN087, the occurrence of a low Q peak (Figure 3) indicates the existence of mesoscopic organization. The long-range structure is

also confirmed by the second and subsequent solvation shells moving at greater distances (Figure 5). The subsequent increase of NMP in the mixtures (PN064, PN05) alters the long-range arrangement. The NMP molecules unlikely slip through the nitrate and ammonium ions. Nevertheless the content of ionic liquid in these mixtures ($x_{PAN} = 0.64$ and 0.5) is such that the long-range structure of the ionic liquid is not completely destroyed, as confirmed by the residual low Q peak (see Figure 3). This suggest that the structure of these mixtures is probably microeterogeneous [28], formed by alternating clusters of NMP and PAN with the anion-cation interaction of ionic liquid preserved. This is easily visible in Figure 7 that shows a typical simulation frame of PN05, in which the mole fraction of PAN is 0.5 and the two compound are in the same amount. A simple inspection of this snapshots reveals some aspects of the mesoscopic organization in the mixture: the trend of the apolar moieties is to cluster inside the ionic liquid structure. This scheme is not dissimilar from the one reported for other related systems, such as EAN-water or EAN-inorganic salt [29, 30]. The main driving force behind microscopic and mesoscopic order is the dichotomy polar versus apolar. This leads to the clustering of the apolar moieties into small domains that are enclosed in the mesh ionic network. At higher NMP content, the low molecules of PAN are indistinguishable mixed with NMP molecules; NMP replaces PAN molecules in the ionic liquid network. PN033 mixture no longer presents a low Q peak. At this concentration, the polar-apolar dualism is no longer sufficient to account for the morphology in terms of a segregated structure. This scenario is confirmed by the thermodinamic data in [5] in which an excess volume for the PAN-NMP system is present, with a minimum at ca. $x_{PAN} = 0.33$.

4. Conclusion

In this work a comparison between the experimental curves of X-ray scattering and the corresponding Molecular Dynamics simulations for a set of seven solutions with with different composition of NMP and PAN is reported. The reached agreement between experimental and theoretical data is good enough to allow us to trace the characteristics of the liquid local structure. As regards the intermolecular interactions, the analysis shows how the struc-

ture of the solution changes varying the concentration of analytes. At high PAN concentration the structure of the mixture is pratically like many other ionic liquids that are arranged in a three-dimensional network seeing locally alternating between ions of opposite sign [31] [32]. At higher NMP content, the structure of the mixture is microheterogeneous. Althoug PAN and NMP mix with each other on a macroscopic scale, they do not mix at microscopic length scale, as shown by the existence of the pre-peak. Both ammonium-nitrate and ammonium-NMP contacts take palce at shorter average distance and this interactions contribute to the internal cohesion of the liquid. The mixing of the two compounds results in the breaking of the long-range structure that the two neat liquids possess individually. In the mixture the short range ion pairs are not affected appreciably: the configuration of the mixture is constituted by aggregates of molecules of PAN and NMP that succeed one another, for which the curve of the diffraction is generated by the contributions of the various domains.

Acknowledgments

We would like to kindly thank *Dr. Lorenzo Gontrani* (Chemistry Department, Sapienza University of Rome) for the fruitful and helpful discussions about MD simulations. **Computational resources were provided by Narten Cluster hpc Facility.**

References

[1] K. R. Seddon, J. Chem. Tech. Biotech. 68 (1997) 351–356.

[2] T. L. Greaves, C. J. Drummond, Chem. Rev. 108 (2008) 206–237.

[3] M. J. Earle, K. R. Seddon, Pure Appl. Chem. 72 (2000) 1391–1398.

[4] N. V. Plechkova, K. R. Seddon, Chem. Soc. Rev. 37 (2008) 123–150.

[5] M. Usula, E. Matteoli, F. Leonelli, F. Mocci, F. C. Marincola, L. Gontrani, S. Porcedda, Fluid Phase Equilib. 383 (2014) 49–54.

[6] S. Porcedda, M. Usula, B. Marongiu, Physical-chemical properties of ionic liquid-containing mixtures, in: The Structure of Ionic Liquids, Springer, 2014, pp. 171–191.

[7] A. Heintz, J. Chem. Thermodyn. 37 (2005) 525–535.

[8] M. Usula, S. Porcedda, F. Mocci, L. Gontrani, R. Caminiti, F. Cesare Marincola, J. Phys. Chem. B 118 (2014) 10493–502.

[9] Y. Murata, K. Nishikawa, Bulletin Chem. Soc. Japan 51 (1978) 411–418.

[10] G. Fritsch, D. A. Keimel, Mater. Sci. Eng. A 134 (1991) 888–892.

[11] C. J. Pings, J. Waser, J. Chem. Phys 48 (1968) 3016–3018.

[12] L. Gontrani, P. Ballirano, F. Leonelli, R. Caminiti, X-ray diffraction studies of ionic liquids: From spectra to structure and back, in: The Structure of Ionic Liquids, Springer, 2014, pp. 1–37.

[13] M. Carbone, R. Caminiti, C. Sadun, J. Mater. Chem. 6 (1996) 1709–1716.

[14] D. A. Case, T. E. Cheatham, T. Darden, H. Gohlke, R. Luo, K. M. Merz, A. Onufriev, C. Simmerling, B. Wang, R. J. Woods, The amber biomolecular simulation programs, J. Comp. Chem. 26 (2005) 1668–1688.

[15] J. Wang, R. M. Wolf, J. W. Caldwell, P. A. Kollman, D. A. Case, J. Comp. Chem. 25 (2004) 1157–1174.

[16] F.-Y. Dupradeau, A. Pigache, T. Zaffran, C. Savineau, R. Lelong, N. Grivel, D. Lelong, W. Rosanski, P. Cieplak, Phys. Chem. Chem. Phys. 12 (2010) 7821–7839.

[17] M. J. Frisch, G. Trucks, H. Schlegel, G. Scuseria, M. Robb, J. Cheeseman, G. Scalmani, V. Barone, B. Mennucci, G. Petersson, al., Gaussian Inc., Wallingford, CT, (2009) *Gaussian 09*, Revision D.01.

[18] E. Bodo, S. Mangialardo, F. Ramondo, F. Ceccacci, P. Postorino, J. Phys. Chem. B 116 (2012) 13878–13888.

[19] M. Campetella, L. Gontrani, F. Leonelli, L. Bencivenni, R. Caminiti, ChemPhysChem 16 (2015) 197–203.

[20] L. Martínez, R. Andrade, E. G. Birgin, J. M. Martínez, J. Comp. Chem. 30 (2009) 2157–2164.

[21] L. Gontrani, R. Caminiti, J. Chem. Phys. 136 (2012) 074505.

[22] R. Caminiti, M. Magini, Chem. Phys. Lett. 54 (1978) 600–602.

[23] M. Macchiagodena, F. Ramondo, A. Triolo, L. Gontrani, R. Caminiti, J. Phys.Chem. B 116 (2005) 13448–13458.

[24] K. Fumino, A. Wulf, R. Ludwig, Angew. Chem. Int. Ed. Engl. 48 (17) (2009) 3184–3186.

[25] R. Hayes, S. Imberti, G. G. Warr, R. Atkin, Phys. Chem. Chem. Phys. 13 (2011) 13544–13551.

[26] R. Atkin, G. G. Warr, J. Phys. Chem. B 112 (2008) 4164–4166.

[27] T. L. Greaves, D. F. Kennedy, S. T. Mudie, C. J. Drummond, J. Phys. Chem. B 114 (2010) 10022–10031.

[28] A. Triolo, O. Russina, H.-J. Bleif, E. Di Cola, J. Phys. Chem. B 111 (2007) 4641–4644.

[29] R. Hayes, S. Imberti, G. G. Warr, R. Atkin, Angew. Chem. Int. Ed. 51 (2012) 7468–7471.

[30] O. Russina, R. Caminiti, T. Méndez-Morales, J. Carrete, O. Cabeza, L. Gallego, L. Varela, A. Triolo, J. Mol. Liquids 205 (2015) 16–21.

[31] R. Hayes, S. Imberti, G. G. Warr, R. Atkin, Phys. Chem. Chem. Phys. 13 (2011) 13544–13551.

[32] O. Russina, A. Triolo, L. Gontrani, R. Caminiti, D. Xiao, L. Hines, R. Bartsch, E. Quitevis, N. Pleckhova, K. Seddon, J. Phys-Cond. Matter 21 (2009) 424121.